# Characterization of dextran particle size: How frit-inlet asymmetrical flow field-flow fractionation (FI-AF4) coupled online with dynamic light scattering (DLS) leads to enhanced size distribution

Laura Marcela Forero Ramirez, Christophe Rihouey, Frédéric Chaubet, Lecerf Didier, Luc Picton

# Characterization of dextran particle size: how Frit-Inlet Asymmetrical Flow Field-Flow Fractionation (FI-AF4) coupled online with dynamic light scattering (DLS) leads to enhanced size distribution.

Laura Marcela Forero Ramirez[a, b, c], Christophe Rihouey[c], Frédéric Chaubet[a, b], Didier Le Cerf[c], Luc Picton[c]±

[a] Laboratory for Vascular Translational Science, UMRS1148, INSERM, Université de Paris, F-75018 Paris, France

[b] Université Sorbonne Paris Nord, F-93430 Villetaneuse, France

[c] Normandie Univ, UNIROUEN, INSA Rouen, CNRS, PBS, UMR6270, 76000 Rouen, France

Corresponding author:

± Correspondence to: Luc Picton (e-mail: luc.picton@univ-rouen.fr)
Tel: (33) (0) 2-35-14-00-71

## HIGHLIGHTS

- An FI-AF4 separation method for dextran nanoparticles was developed.
- FI-AF4 coupled to the DLS detector showed the whole distribution of nanoparticles.
- The enhanced resolution of the FI-AF4 technique was proven.
- Batch-mode DLS was not suitable and provided misleading information.
- The good reproducibility of the particle preparation method was demonstrated.


## ABSTRACT

Accurate determinations of particle size and particle size distribution (PSD) are essential to achieve the clinical translation of medical nanoparticles (NPs). Herein, dextran-based NPs produced via a water-in-oil emulsification/crosslinking process and developed as nanomedicines were studied. NPs were first characterized using traditional batch-mode techniques as dynamic light scattering (DLS) and laser diffraction. In a second step, their analysis by frit-inlet asymmetrical flow field-flow fractionation (FI-AF4) was explored. The major parameters of the AF4 procedure, namely, crossflow, detector flow, crossflow decay programming and relaxation time were set up. The sizes of the particle fractions eluted under optimized conditions were measured using DLS as an online detector. We demonstrate that FI-AF4 is a powerful method to characterize dextran-NPs in the 200 nm -1 µm range. It provided a more realistic and comprehensive picture of PSD, revealing its heterogenous character and clearly showing the ratio of different populations in the sample, while batch-mode light scattering techniques only detected the biggest particle sizes.



**Keywords**

Frit-Inlet Asymmetrical Flow Field-Flow Fractionation (FI-AF4)

Dextran

Nanoparticles

Dynamic Light Scattering (DLS)

Size-based separation

## 1. Introduction

Nanoparticle (NP) based technologies have found numerous applications in the biomedical field, ranging from controlled and targeted delivery of therapeutic compounds to imaging, diagnostics, and monitoring of disease processes [1,2]. Once systematically administered, the fate and biological performance of NPs rely on their physicochemical properties: shape, surface chemistry, charge and, in particular, their size [3]. Particle size and particle size distribution (PSD) appear to dictate NP blood circulation half-life [3,4], biodistribution throughout the body and within specific organs [4,5], tumour penetration [6,7], cellular uptake mechanism [8,9], targeting [10], toxicity [11], therapeutic index [12] and even contrast properties [13]. The development of NPs with narrow and controlled PSD as well as reliable routine methods for their quality control and characterization are therefore of key importance for clinical translation.

Several methods are available for size and PSD analysis. Among them, scanning and transmission electron microscopy (SEM and TEM) approaches are commonly used for direct visualization of NP shape, surface, and geometric size [14,15]. Nevertheless, size assessment is often laborious and time consuming, as a very large number of particles must be observed to obtain statistically significant PSD information [16,17]. Moreover, under sample preparation conditions (dried state and high-energy electron source), the observed size and morphology may not be representative of those in biological aqueous environments [18]. In this regard, dynamic light scattering (DLS), also called quasi-elastic light scattering (QELS), has become the standard approach to determine NP size in suspension. DLS measures the translational diffusion coefficient of NPs in dispersing media by quantifying dynamic fluctuations in scattered light [19,20]. This information is then converted into a particle size by applying the Stokes-Einstein equation. When used in batch-mode, DLS allows accurate, simple, and fast characterization of monomodal NPs in different dispersing media while

77 requiring limited sample quantities. However, size resolution can be significantly
78 compromised in the case of complex mixtures or highly dispersed samples.

79 One way to overcome this drawback is to introduce a fractionation step to separate the
80 particles, according to their size, prior to DLS detection. In asymmetrical flow field flow
81 fractionation (AF4) method, this separation can be achieved into a narrow, opened, and
82 unpacked channel [21–25]. Briefly, a single carrier flow is pumped from the channel inlet and
83 split into both the channel flow and the crossflow (Figure 1). The channel flow displays a
84 parabolic velocity profile and carries NPs to the channel outlet where they are detected. The
85 crossflow, which moves from the top to the bottom of the channel, forces NPs down to the
86 accumulation wall (an ultrafiltration membrane overlaying a porous frit). Finally,-natural NP
87 diffusion counteracts the crossflow field, allowing size fractionation. Due to their higher
88 translational diffusion coefficients, smaller particles tend to reach an equilibrium position
89 higher up in the channel. They thus experience a faster channel flow velocity and are eluted
90 earlier than larger particles.

91 Coupled with downstream detectors such as refractive index (RI), multiangle light scattering
92 (MALS), ultraviolet-visible spectrophotometry (UV-Vis) and DLS, AF4 has been effectively
93 used for the analysis and characterization of different NPs including liposomes [26], lipid-
94 based NPs [27,28], polymeric NPs [14,23,29–31], metallic NPs [32,33], and metal oxide NPs
95 [34–36]. To the best of our knowledge, very few examples have dealt with pure
96 polysaccharide NPs, and almost all of them were made of chitosan [37–39]. It is well known
97 that a new and specific AF4 method needs to be established for each kind of NP depending on
98 its surface properties, composition, average size, and size distribution. Herein, we present the
99 development and optimization of a separation method for dextran-based NPs produced via a
100 simple water-in-oil emulsification/crosslinking process. The potential of such NPs as MRI
101 contrast agent carriers for atherothrombosis detection was recently reported [40]. AF4 could

provide deeper characterizations of their average size, PSD and preparation method reproducibility, which are essential to complete their preclinical development. The main parameters influencing AF4 separation, including spacer height, crossflow rate and relaxation time, were studied. The optimized procedure was then applied to assess particle size and PSD. AF4 results were finally compared against batch-mode DLS data to draw conclusions about the suitability of the latter as a routine quality control technique. Orthogonal methods, such as TEM, SEM, and confocal microscopy, were performed to support the results.

## 2. Materials and methods

### *2.1 Chemicals*

Dextran T70 ($\overline{M}_n$= 55 000 g/mol, Đ = 1.12) was purchased from Pharmacosmos (Holbæk, Denmark). Trisodium trimetaphosphate (STMP) was obtained from Sigma Aldrich (Saint-Quentin-Fallavier, France). Fluorescein isothiocyanate-dextran (FITC-dextran, $\overline{M}_w$ = 70 000 g/mol) was purchased from TdB Consultancy (Uppsala, Sweden). Polyglycerol polyricinoleate (PGPR 4150) was a gift from Palsgaard SAS (Lyon, France). Sunflower oil (Lesieur, France) is a mixture of saturated fatty acids (palmitic acid ~5 wt%- and stearic acid ~6 wt%) and unsaturated fatty acids (mainly oleic acid ~37 wt% and linoleic acid ~51 wt%). All materials were of analytical grade and were used without further purification. Ultrapure water was used throughout this work.

### *2.2 Dextran-NPs synthesis*

Dextran T70 particles were obtained via a water-in-oil emulsification-crosslinking method as previously described [40]. The typical experimental conditions were as follows: 1.2 g of dextran and 1.4 g of NaCl were solubilized in 4 mL of water. Then, 1.2 g of this solution was

125 mixed with 120 µL of NaOH (10 M) and 240 µL of the crosslinking agent trisodium
126 trimetaphosphate (STMP) (30% (w/v) in water). A total of 600 µL of the mixture was slowly
127 injected into 30 mL of sunflower oil containing 6.0% (w/v) polyglycerol polyricinoleate
128 (PGPR) as an emulsion stabilizer and dispersed with a homogenizer at 24,000 rpm for 4 min
129 (IKA T18 Basic equipped with a dispersing element IKA S 18 N-19 G, Germany). The
130 resulting emulsion was then put in an oil bath (50 °C) wherein the crosslinking step took place
131 for 20 min. Polysaccharide particles were recovered by ultracentrifugation (15,000 x g,
132 45 min), washed once with 1X PBS twice with SDS (0.04% (w/v)) and four times with water.
133 The resulting pellets were resuspended in water and stored at 4 °C until use.

134 *2.3 Dynamic light scattering (DLS) and* ζ-potential

135 Batch DLS measurements were performed using a Malvern Zetasizer Ultra instrument
136 (Worcestershire, UK) equipped with a 633 nm He-Ne laser. Particles were analysed as
137 synthesized without prior filtration to avoid material losses, e.g., aggregates and large
138 populations (previous filtration with a 1.2 µm filter did not affect the size distribution results).
139 The particle concentration was fixed to 0.5 mg/mL to obtain an attenuator factor of 6 or 7.
140 Experimental measurements were performed with a fixed 173° scattering angle at 25°C after
141 an equilibration step of 2 min. Each sample was recorded in triplicate using at least 20 data
142 sets acquired for 10 s each. The correlation function was analysed–by the general-purpose
143 method (using a nonnegative least square algorithm) for derivation of the intensity-weighted
144 particle size distribution, intensity-weighted mean diameter ($D_{h\text{-}DLS}$) and polydispersity index
145 (PDI). Average values of replicates (n=3) are reported.

146 The ζ-potential was determined in 1 mM KCl at 25°C with the same instrument. The
147 measurements of the electrophoretic mobility were converted to ζ-potential (mV) using the

148 Smoluchowski approximation. Average values of three consecutive measurements (n=3) are
149 reported.

150

151 *2.4 Laser diffraction measurements*

152 Batch laser diffraction measurements were performed using a Mastersizer 3000 (Malvern
153 Instruments, UK). The refractive indexes were 1.20 for the dispersed phase (dextran-NPs) and
154 1.330 for the dispersant (water). An absorption index of 0.01 was applied. Volume and
155 number-based PSDs obtained by Mie theory are reported together with the corresponding
156 median diameters (D50v and D50n). The width of the PSD is commonly described by the
157 sizes of the finest (D10) and coarsest (D90) fractions. Using the same convention as D50,
158 10% of the total particles have a diameter below D10, while 90% have a diameter below D90.
159 Average values of three consecutive measurements (n=3) are given.

160 *2.5 Frit Inlet Asymmetrical Flow-Field Flow Fractionation (FI-AF4)*

161 Flow-field flow fractionation of polysaccharide NPs was carried out in a frit-inlet
162 asymmetrical channel (270 mm length, Wyatt technology, CA, USA*)* linked to: i) an Eclipse
163 AF4 flow control module (Wyatt technology, CA, USA), ii) a differential refractive index
164 detector (RID-10A, Shimadzu, Japan), iii) a multiangle light scattering detector (MALS,
165 Dawn-EOS, Wyatt technology, CA, USA), and iv) a quasi-elastic light scattering detector
166 (Wyatt-QELS (or DLS), Wyatt technology, CA, USA) connected to the MALS photodiode at
167 an angle of 111°. The accumulation wall was an ultrafiltration membrane of regenerated
168 cellulose with a 10-kDa cut-off. Two spacers were used: 350 µm and 490 µm. An isocratic
169 pump (LC-10A, Shimadzu, Japan) equipped with an in-line vacuum degasser (DGU 20A3,
170 Shimadzu, Japan) and an autosampler (SIL-20A, Shimadzu, Japan) provided the carrier flow
171 and handled the sample injection into the channel, respectively. The carrier liquid was

composed of Milli-Q water containing 0.02% $NaN_3$ prefiltered at 0.1 µm. The particle concentration was set to 0.5 mg/mL and the injection volume was 10 µL. Analyses were performed at room temperature. The collected data were analyzed using the Astra 6.1.7. software package. The weight-based size distribution was calculated by using the hydrodynamic diameter acquired by DLS and sample concentration measured by the RI detector.

*2.6 SEM, TEM and Confocal Microscopy*

Particles were visualized by transmission electron microscopy (TEM, Tecnai 12, 80 kV; FEI; Hillsboro, OR, USA), scanning electron microscopy (SEM, Philips XL30 ESEM-FEG, Netherlands) and confocal microscopy (Zeiss LSM 780 with 63× oil objective, Carl Zeiss Microscopy, Germany). For TEM observation, 3 µL of particle suspension was dropped onto a 400-mesh copper grid and positively stained with uranyl acetate (1% (w/v)) and allowed to air-dry at room temperature. For SEM images, one drop of particle suspension was dropped onto a silicon wafer, air-dried and coated with a thin layer of gold before observation.

## 3. Results and discussion

### 3.1 Particles preparation and batch mode characterization

Dextran-NPs were prepared by a water-in-oil emulsion/crosslinking method using STMP as a crosslinking agent. The optimization of this method is described elsewhere [40]. Due to the anionic charges brought by STMP, dextran-NPs exhibited a negative zeta potential (-28±3 mV) and behaved as three-dimensional and hydrophilic polymeric networks able to swell and hold a great amount of water (Figure 2A). The water content of dextran-NPs dispersed in Milli-Q water was estimated to be approximately 98% of the wet weight.

Dextran-NP size was first characterized in batch mode by DLS. As shown in Figure 2B, dextran-NPs exhibited a monomodal profile, with particle sizes ranging from 350 nm to 1.6

196 µm, an intensity-weighted mean diameter ($D_{h\text{-}DLS}$) of 760±13 nm and a polydispersity index
197 (PDI) of 0.17±0.02. These results were consistent with a PSD of moderate width. As stated in
198 the international standard (ISO 22412:2017), intensity-based results are the most reliable
199 parameters provided by DLS to describe particle size and PSD. Nevertheless, for comparison
200 purposes, the intensity distribution was converted into volume and number distributions using
201 Mie theory. This theory assumes that all the particles are spherical and that the optical
202 properties of both the particles, and the dispersing medium, are known. As expected, the
203 number PSD shifted towards smaller sizes with a maximum peak size of approximately 750
204 nm (Figure 2B). In contrast, the volume PSD favoured larger particles with a peak maximum
205 of approximately 1 µm.

206 Laser diffraction was used as complementary batch sizing technique. In this case, particles
207 cause light diffraction with a scattering angle that depends on particle size under the
208 assumption that the particles are spherical. In principle, small particles will scatter light at
209 large angles while large particles will scatter light at small angles [41]. The scattering pattern
210 produced by the sample could once again be directly related to PSD by applying Mie theory.
211 Laser diffraction provided both volume and number size distributions of dextran-NPs (Figure
212 2C). As for DLS analysis, only one population was detected. The volume and number-median
213 diameters (D50v and D50n) of dextran-NPs were evaluated to be 910±10 nm and 720±12
214 nm, respectively, which closely corresponds to the previous observations by DLS. On a
215 volume basis, D10v = 630 nm and D90v = 1.2 µm whereas in number one, D10n = 530 nm
216 and D90n = 1.0 µm.

217 Both DLS and laser diffraction suggested a quite homogeneous batch with most of the
218 particles in the submicronic size range. To confirm these results and validate the use of batch-
219 mode light scattering methods as fast and simple quality control techniques, dextran-NPs were

analysed by AF4. The use of a fractionation step, which separates the particles according to their size, and continuous online detection by DLS were expected to provide a PSD with higher resolution.

### 3.2 AF4 method development

#### 3.2.1 Channel characteristics

When NPs are injected into an AF4 system, a relaxation process occurs prior to separation. This process allows NPs to reach their diffusion-dependent equilibrium positions and thus different velocity streamlines of the parabolic flow profile. In a conventional AF4 channel, relaxation takes place during a focusing step in which the sample is concentrated in a relatively narrow band near to the injection point by two counterdirected flows [42]. However, the focusing process may cause sample aggregation, mass losses due to adsorption into the accumulation wall, incomplete relaxation due to the high local concentration or baseline fluctuations because of the rapid flow rate changes [43–45]. In this study, a long AF4 channel (270 mm) equipped with a frit inlet (FI-AF4) was used (Figure 1). The focusing step was completely avoided, and the sample was relaxed hydrodynamically as it entered–the channel by the compressing effect of the frit inlet flow [45,46]. The FI-AF4 channel has been shown to allow for a higher injection mass than the conventional channel while limiting overloading effects and normally leading to higher recoveries [42].

In an AF4 system, particles can be separated following two different modes of retention. We have already described the so-called normal mode where fractionation is governed by Brownian motion and smaller particles elute earlier than larger particles. Nevertheless, beyond a certain size limit, the diffusive transport opposing the crossflow field is negligible, and the elution becomes dependent on the position of the particles centre of mass in the parabolic flow profile [47]. In this case, larger particles protruding farther into the channel

experience higher velocities and are eluted before the smaller particles [48,49]. This is referred to as the steric mode. Between the two modes, in the so-called steric transition region, two groups of particles having different sizes are eluted together, one by the normal mode and the other by the steric mode [50,51]. This makes it difficult to accurately interpret size data, especially when the sample has a broad size distribution. Thus, AF4 separation conditions need to be adjusted to ensure that the entire population of the sample is governed by only one kind of elution mechanism.

The crossover between normal and steric modes, also called the steric inversion diameter, depends on the channel dimensions, field strength and flow rates. Steric inversion diameters of 0.2-0.5 µm were reported by Dou et al. [52] for polystyrene particles eluted in a conventional AF4 channel using a constant-crossflow method. Kim et al. [53] investigated the steric transition of polystyrene particles in an FI-AF4 channel. They demonstrated that the steric inversion diameter can be increased by programming the crossflow field and by increasing the channel thickness. Values of 0.7, 1.1 and 1.8 µm were determined for channel spacers of 190, 350 and 490 µm, respectively. Based on these studies and because of the expected dextran-NPs size (~760 nm), spacers heights equal to or above 350 µm appeared suitable to elute all NP batches in the normal mode. However, initial screening performed with a spacer of 350 µm did not lead to convenient separation. The spacer thickness was thus increased to 490 µm for the optimization approach described below.

### 3.2.2 AF4 flow settings

The typically applied AF4 sequence is summarized in Figure 3. Step 1 allowed system equilibration at the desired flow rates. Injection and relaxation of the sample took place simultaneously in step 2 under a constant initial crossflow rate. The actual sample separation and elution occurred in steps 3 and 4 after a gradual decrease in the crossflow field. In step 5,

the crossflow was set to zero to investigate whether a fraction of the sample experienced strong retention in the channel. All separations were performed at room temperature using Milli-Q water as liquid carrier. A regenerated cellulose membrane with a cut-off of 10 kDa was chosen as the accumulation wall. Electrostatic repulsions between the negative surfaces of both the membrane and dextran-NPs were expected to prevent potential attachment or adsorption of NPs on the membrane. A dextran-NP mass of 5 µg was injected to obtain an exploitable signal in all detectors.

The frit inlet flow (FF) and the crossflow (CF) are the key parameters determining the resolution and separation quality of an FI-AF4 system. Previous studies have shown that efficient hydrodynamic relaxation can be obtained using a high ratio of the FF rate to the sample injection flow rate (IF). FF/IF values greater than or equal to 20 are normally recommended [53–55]. Since there is no incoming CF in an asymmetrical channel, the sum of the channel flow and the outgoing CF corresponds to the FF (Figure 1). Following the recommendations of the instrument supplier, the injection and channel flow rates were set to 0.1 and 0.6 mL/min, respectively. Both the field strength and the FF rate were varied simultaneously by using different initial CFs. For these experiments, the sample was injected and relaxed for 10 min (step 2) at the set CF rate. A linear decay of the CF in 1 min (step 3) was found to be the better choice for field strength programming.

As shown in light scattering (LS) fractograms (Figure 4), a too low initial CF (0.1 mL/min, FF/IF= 7) led to a high number of unfractionated particles eluting prematurely in the so-called void peak. This peak disappeared for CF rates equal to or above 0.2 mL/min (FF/IF= 8). Nevertheless, when using too high CFs, the baseline could not be reached within 60 min of the sample run. At these crossflow fields (1.0 mL/min and 2.2 mL/min) and the resulting FF/IF ratios (16 and 28, respectively), particles were probably compressed too close to the

accumulation wall and were subsequently highly retained by increased particle-membrane interactions. A CF rate of 0.3 mL/min, corresponding to an FF rate of 0.9 mL/min and an FF/IF ratio of 9, was ultimately chosen because it was high enough to obtain suitable particle separation but low enough to provide a proper shape peak. Under these conditions, a retention time of 18 min and a peak width of 20 min were obtained.

To examine the effect of the relaxation time, CF was fixed to 0.3 mL/min, and the duration of step 2 was varied from 5 to 15 minutes. In all cases, particle elution started in step 4 after the end of the relaxation phase and CF linear decay.–Ten minutes was found to be the optimal time. A further rise in relaxation time did not result in better separation quality. The effect of the CF decay pattern (step 3) was also explored. Linear, stepwise, exponential and power crossflow decays with decay times ranging from 1 to 20 minutes were tested. Nevertheless, a 1-minute linear decay allowed for the best compromise between size resolution and overall run duration.

A screening of the channel flow rate between 0.5 and 0.8 mL/min was also performed, and all other run conditions were the same. It was observed that the axial flow velocity should be as low as possible to provide enough residence time for suitable sample relaxation. While the overall dextran-NPs were eluted in normal mode at 0.5 and 0.6 mL/min, a combination of both steric and normal retention mechanisms was observed at higher channel flow rates (see supporting information, Figure S1). A 0.6 mL/min volumetric flow rate was ultimately selected, which resulted in better resolution and narrower elution peaks. Table 2 summarizes the parameters of the final AF4 separation method.

### 3.2.3 Dextran-NPs size distribution by FI-AF4

315 The hydrodynamic size of fractionated dextran-NPs was measured with an in-line DLS
316 detector at an angle of 110°. The resulting fractogram and size distribution profile are
317 depicted in Figure 5A. The optimized FI-AF4 method allowed the detection of NPs with sizes
318 ranging from 260 nm to 1 µm while maintaining normal separation mode. An intensity-
319 weighted mean diameter of 340 nm was estimated. The AF4 method showed good
320 reproducibility, as the relative standard deviation of the mean diameter was below 3.0% (n =
321 3). DLS signal showed a single monomodal distribution, although a small shoulder is
322 apparent at higher particle sizes. Weight-based PSD, deduced from both QELS and RI data,
323 confirmed the presence of a major population of approximately 320 nm and a long tail
324 between 400 nm and 1 µm (Figure 5B). The relative proportion of both main peak and tail
325 was assessed from the cumulative weight-based distribution. Seventy percent of dextran-NPs
326 were found to have a diameter equal to or below 400 nm, whereas particles with a diameter
327 between 400 nm and 1 µm represented only 30% of the sample. The intensity correlation
328 functions of particle fractions obtained at different elution times are depicted in Figure 5C. In
329 all cases, cumulant analysis provided a good fit of the single exponential decay, attesting to
330 the quality of the data acquired from the DLS detector.

331 **3.3 FI-AF4 vs. batch-mode DLS**

332 Batch-mode DLS and FI-AF4 analysis provided quite different pictures of dextran-NP size
333 distribution. On the one hand, DLS measurements of unfractionated particles resulted in an
334 average diameter of 760 nm in combination with a monomodal PSD. On the other hand, FI-
335 AF4 delivered the whole size distribution of the sample between 260 nm and 1 µm with a
336 mean size that was almost two times lower (340nm) and a long-tailed. To discriminate
337 between the two techniques, dextran-NPs were directly visualized by TEM, SEM and
338 confocal microscopy. The resulting micrographs, depicted in Figure 6, clearly supported FI-
339 AF4 analysis. The heterogeneity of the dextran-NP batch became evident together with the

coexistence of particles of very different sizes. In addition, all techniques confirmed the obtention of spherical shaped NPs, and diameters between approximately 300 nm and 1 µm were observed by confocal microscopy, where particles were imaged under hydrated conditions.

Batch-mode DLS failed to differentiate the dextran-NPs mixed population and delivered a size distribution skewed towards larger particles visibly present to a lower extent (Figure 6). These findings were consistent with comparative studies performed on multimodal dispersions prepared intentionally by mixing at least three particle sizes. Mixtures of gold NPs (5-60 nm) [56], pegylated gold NPs (30-90 nm) [57] and silver NPs (30-100 nm) [58,59] were examined, and similar conclusions were drawn in all cases. While AF4 was able to discriminate and quantify the different populations due to sufficient resolution, batch-DLS gave one broad peak weighted towards the biggest particles in the sample. In another work, Varenne et al. [23] reported a complete evaluation of the PSD of dextran-covered poly(isobutylcyanoacrylate) NPs. Nine different sizing techniques were used, including DLS, SEM, TEM and AF4. DLS did not reveal the complexity of the PSD, showing only one population of NPs of approximately 200 nm with narrow polydispersity. In contrast, AF4 identified a multimodal dispersion with four peaks of significantly different sizes (97, 168, 417 and 446 nm), in agreement with observations made on TEM and SEM micrographs. These examples highlighted the limits of batch-mode DLS in regard to resolving complex samples. This lack of sensitivity, leading in most cases to the overestimation of particle size, appear to be an inherent artifact of DLS and is directly related to its measurement principle. The Rayleigh approximation states that the intensity of the scattered light is proportional to the particle diameter to a power of six [20]. This means that NPs of 50 nm scatter one million times as much light as NPs of 5 nm. Consequently, in batch-mode some larger particles or aggregates can mask the presence of smaller particles, ultimately biasing the DLS response. In

addition, DLS requires particles different in size by at least a factor of 3 to offer enough peak resolution. This makes difficult to analyse polydisperse samples with particles of closer sizes as is the case of Dextran-NPs [60]. In those situations, particle fractionation prior to DLS detection appeared essential to obtain reliable PSD information.

### 3.4 Batch to batch reproducibility

Reproducible manufacturing of nanomedicines is one of the key parameters determining their successful translation into commercial products. Batch-to batch consistency should thus be checked from the early stages of development, since significant variation of the PSD between batches could result in distinct biological properties [61]. In this work, four batches of dextran-NPs were prepared using the same protocol and their PSD was determined by FI-AF4 and batch-mode DLS. As shown in Figure 7, the manufacturing process of dextran-NPs appeared to be highly reproducible. No significant differences were detected in the weight-based size distribution given by FI-AF4, except for batch B where particles below 400 nm were present to a lesser extent. As expected, batch-mode DLS gave similar monomodal distributions systematically biased towards larger particles, with intensity-weighted mean diameters between 700 and 760 nm and PDI values below or equal to 0.18 (Table 2).

With all this evidence, we can conclude that batch-mode DLS is not suitable for dextran-NPs characterization. Conversely, FI-AF4 not only was able to measure the PSD of dextran-NPs with high resolution but also allowed us to resolve small changes in size between different batches. FI-AF4 can thus be considered a promising technique for the synthesis optimization and quality control of this nanosystem.

## 4. Conclusion

Polysaccharide-based nanoparticles are being developed as promising imaging and therapeutic tools for multiple diseases. Their translation to commercial products involves deep characterization of their physicochemical properties, especially their size and size distribution. In this study we developed and validated an FI-AF4 protocol allowing accurate and reproducible characterization of dextran-NPs in the 200 nm -1 µm range. The results presented here once again highlight the inherent limitations of batch-mode DLS. Although widely used in laboratories for an initial quick and easy check of new samples, DLS data should be interpreted carefully and systematically contrasted with other sizing techniques, to avoid drawing misleading conclusions. In this respect, FI-AF4 was found to be a valuable technique that is able to provide ~~a~~ realistic and complete knowledge of dextran-NPs. Even if FI-AF4 method development is more laborious and time consuming, once established, it becomes a robust, accurate and sensitive tool for the routine characterization of complex nanosystems.

**Acknowledgment**

The authors express their highest gratitude to Christine Choqueux (LVTS, Paris, France) and UTC (Compiègne, France) for the SEM images and to Samira Benadda and CRI U1149 imaging facilities for confocal imaging training. We also thank Rémi Le Borgne and the ImagoSeine facility, member of the France BioImaging infrastructure supported by grant ANR-10-INBS-04 from the French National Research Agency, for their valuable help with TEM images.

This work was supported by INSERM, Université de Paris, Université Paris 13, UMS34 FRIM and Université de Rouen Normandie, and received the financial support from the ANR-16-CE18-0031 NANOPACT. The authors thank the Normandy region and the European Union for their financial support in the purchase of equipment (project FInnS).

## CRediT author statement

**Laura Marcela Forero Ramirez:** Conceptualization, Investigation, Methodology, Formal analysis, Writing - original draft. **Christophe Rihouey:** Conceptualization, Investigation, Methodology**. Frédéric Chaubet:** Project administration, Funding acquisition**. Didier Le Cerf:** Conceptualization, Project administration, Funding acquisition, Supervision, Validation, Writing - review & editing**. Luc Picton:** Conceptualization, Project administration, Funding acquisition, Supervision, Validation, Writing - review & editing**.**

## References


[1] K. McNamara, S.A.M. Tofail, Nanoparticles in biomedical applications, Adv. Phys. X. 2 (2017) 54–88. https://doi.org/10.1080/23746149.2016.1254570.

[2] B.L. Banik, P. Fattahi, J.L. Brown, Polymeric nanoparticles: the future of nanomedicine: Polymeric nanoparticles, Wiley Interdiscip. Rev. Nanomed. Nanobiotechnol. 8 (2016) 271–299. https://doi.org/10.1002/wnan.1364.

[3] X. Duan, Y. Li, Physicochemical Characteristics of Nanoparticles Affect Circulation, Biodistribution, Cellular Internalization, and Trafficking, Small. 9 (2013) 1521–1532. https://doi.org/10.1002/smll.201201390.

[4] F. Alexis, E. Pridgen, L.K. Molnar, O.C. Farokhzad, Factors Affecting the Clearance and Biodistribution of Polymeric Nanoparticles, Mol. Pharm. 5 (2008) 505–515. https://doi.org/10.1021/mp800051m.

[5] C. He, Y. Hu, L. Yin, C. Tang, C. Yin, Effects of particle size and surface charge on cellular uptake and biodistribution of polymeric nanoparticles, Biomaterials. 31 (2010) 3657–3666. https://doi.org/10.1016/j.biomaterials.2010.01.065.

[6] Q. Sun, T. Ojha, F. Kiessling, T. Lammers, Y. Shi, Enhancing Tumor Penetration of Nanomedicines, Biomacromolecules. 18 (2017) 1449–1459. https://doi.org/10.1021/acs.biomac.7b00068.

[7] M.J. Ernsting, M. Murakami, A. Roy, S.-D. Li, Factors controlling the pharmacokinetics, biodistribution and intratumoral penetration of nanoparticles, J. Controlled Release. 172 (2013) 782–794. https://doi.org/10.1016/j.jconrel.2013.09.013.

[8] S.E.A. Gratton, P.A. Ropp, P.D. Pohlhaus, J.C. Luft, V.J. Madden, M.E. Napier, J.M. DeSimone, The effect of particle design on cellular internalization pathways, Proc. Natl. Acad. Sci. 105 (2008) 11613–11618. https://doi.org/10.1073/pnas.0801763105.

[9] N. Hoshyar, S. Gray, H. Han, G. Bao, The effect of nanoparticle size on *in vivo* pharmacokinetics and cellular interaction, Nanomed. 11 (2016) 673–692. https://doi.org/10.2217/nnm.16.5.

[10] R. Zein, W. Sharrouf, K. Selting, Physical Properties of Nanoparticles That Result in Improved Cancer Targeting, J. Oncol. 2020 (2020) 1–16. https://doi.org/10.1155/2020/5194780.

[11] M.V.D.Z. Park, A.M. Neigh, J.P. Vermeulen, L.J.J. de la Fonteyne, H.W. Verharen, J.J. Briedé, H. van Loveren, W.H. de Jong, The effect of particle size on the cytotoxicity, inflammation, developmental toxicity and genotoxicity of silver nanoparticles, Biomaterials. 32 (2011) 9810–9817. https://doi.org/10.1016/j.biomaterials.2011.08.085.

[12] J.W. Hickey, J.L. Santos, J.-M. Williford, H.-Q. Mao, Control of polymeric nanoparticle size to improve therapeutic delivery, J. Controlled Release. 219 (2015) 536–547. https://doi.org/10.1016/j.jconrel.2015.10.006.

[13] E.D. Smolensky, H.-Y.E. Park, Y. Zhou, G.A. Rolla, M. Marjańska, M. Botta, V.C. Pierre, Scaling laws at the nanosize: the effect of particle size and shape on the magnetism and relaxivity of iron oxide nanoparticle contrast agents, J. Mater. Chem. B. 1 (2013) 2818. https://doi.org/10.1039/c3tb00369h.

[14] J. Ehrhart, A.-F. Mingotaud, F. Violleau, Asymmetrical flow field-flow fractionation with multi-angle light scattering and quasi elastic light scattering for characterization of poly(ethyleneglycol-b-ε-caprolactone) block copolymer self-assemblies used as drug carriers for photodynamic therapy, J. Chromatogr. A. 1218 (2011) 4249–4256. https://doi.org/10.1016/j.chroma.2011.01.048.

[15] A. Zattoni, B. Roda, F. Borghi, V. Marassi, P. Reschiglian, Flow field-flow fractionation for the analysis of nanoparticles used in drug delivery, J. Pharm. Biomed. Anal. 87 (2014) 53–61. https://doi.org/10.1016/j.jpba.2013.08.018.

[16] S.B. Rice, C. Chan, S.C. Brown, P. Eschbach, L. Han, D.S. Ensor, A.B. Stefaniak, J. Bonevich, A.E. Vladár, A.R.H. Walker, J. Zheng, C. Starnes, A. Stromberg, J. Ye, E.A. Grulke, Particle size distributions by transmission electron microscopy: an interlaboratory comparison case study, Metrologia. 50 (2013) 663–678. https://doi.org/10.1088/0026-1394/50/6/663.

[17] W.D. Pyrz, D.J. Buttrey, Particle Size Determination Using TEM: A Discussion of Image Acquisition and Analysis for the Novice Microscopist, Langmuir. 24 (2008) 11350–11360. https://doi.org/10.1021/la801367j.

[18] P. Reschiglian, D.C. Rambaldi, A. Zattoni, Flow field-flow fractionation with multiangle light scattering detection for the analysis and characterization of functional nanoparticles, Anal. Bioanal. Chem. 399 (2011) 197–203. https://doi.org/10.1007/s00216-010-4197-3.

[19] S. Falke, C. Betzel, Dynamic Light Scattering (DLS): Principles, Perspectives, Applications to Biological Samples, in: A.S. Pereira, P. Tavares, P. Limão-Vieira (Eds.), Radiat. Bioanal., Springer International Publishing, Cham, 2019: pp. 173–193. https://doi.org/10.1007/978-3-030-28247-9_6.

[20] J. Stetefeld, S.A. McKenna, T.R. Patel, Dynamic light scattering: a practical guide and applications in biomedical sciences, Biophys. Rev. 8 (2016) 409–427. https://doi.org/10.1007/s12551-016-0218-6.

[21] F.A. Messaud, R.D. Sanderson, J.R. Runyon, T. Otte, H. Pasch, S.K.R. Williams, An overview on field-flow fractionation techniques and their applications in the separation and characterization of polymers, Prog. Polym. Sci. 34 (2009) 351–368. https://doi.org/10.1016/j.progpolymsci.2008.11.001.

[22] W. Fraunhofer, G. Winter, The use of asymmetrical flow field-flow fractionation in pharmaceutics and biopharmaceutics, Eur. J. Pharm. Biopharm. 58 (2004) 369–383. https://doi.org/10.1016/j.ejpb.2004.03.034.

[23] F. Varenne, A. Makky, M. Gaucher-Delmas, F. Violleau, C. Vauthier, Multimodal Dispersion of Nanoparticles: A Comprehensive Evaluation of Size Distribution with 9 Size Measurement Methods, Pharm. Res. 33 (2016) 1220–1234. https://doi.org/10.1007/s11095-016-1867-7.

[24] L. Picton, I. Bataille, G. Muller, Analysis of a complex polysaccharide (gum arabic) by multi-angle laser light scattering coupled on-line to size exclusion chromatography and flow field flow fractionation, Carbohydr. Polym. 42 (2000) 23–31. https://doi.org/10.1016/S0144-8617(99)00139-3.

[25] C. Duval, D. Le Cerf, L. Picton, G. Muller, Aggregation of amphiphilic pullulan derivatives evidenced by on-line flow field flow fractionation/multi-angle laser light scattering, J. Chromatogr. B. Biomed. Sci. App. 753 (2001) 115–122. https://doi.org/10.1016/s0378-4347(00)00517-x.

[26] S.M. Ansar, T. Mudalige, Characterization of doxorubicin liposomal formulations for size-based distribution of drug and excipients using asymmetric-flow field-flow fractionation (AF4) and liquid chromatography-mass spectrometry (LC-MS), Int. J. Pharm. 574 (2020) 118906. https://doi.org/10.1016/j.ijpharm.2019.118906.

[27] F. Caputo, J. Clogston, L. Calzolai, M. Rösslein, A. Prina-Mello, Measuring particle size distribution of nanoparticle enabled medicinal products, the joint view of EUNCL and NCI-NCL. A step by step approach combining orthogonal measurements with increasing complexity, J. Controlled Release. 299 (2019) 31–43. https://doi.org/10.1016/j.jconrel.2019.02.030.

[28] K. Jores, W. Mehnert, M. Drechsler, H. Bunjes, C. Johann, K. Mäder, Investigations on the structure of solid lipid nanoparticles (SLN) and oil-loaded solid lipid nanoparticles by photon correlation spectroscopy, field-flow fractionation and transmission electron microscopy, J. Controlled Release. 95 (2004) 217–227. https://doi.org/10.1016/j.jconrel.2003.11.012.

[29] C. Scherer, S. Noskov, S. Utech, C. Bantz, W. Mueller, K. Krohne, M. Maskos, Characterization of Polymer Nanoparticles by Asymmetrical Flow Field Flow Fractionation (AF-FFF), J. Nanosci. Nanotechnol. 10 (2010) 6834–6839. https://doi.org/10.1166/jnn.2010.2973.

[30] D. Le Cerf, A.S. Pepin, P.M. Niang, M. Cristea, C. Karakasyan-Dia, L. Picton, Formation of polyelectrolyte complexes with diethylaminoethyl dextran: Charge ratio and molar mass effect, Carbohydr. Polym. 113 (2014) 217–224. https://doi.org/10.1016/j.carbpol.2014.07.015.

[31] D. Le Cerf, S. Simon, J.-F. Argillier, L. Picton, Contribution of flow field flow fractionation with on line static and dynamic light scattering to the study of hydrosoluble polyelectrolyte complexes, Anal. Chim. Acta. 604 (2007) 2–8. https://doi.org/10.1016/j.aca.2007.06.012.

[32] M. Hansen, M.C. Smith, R.M. Crist, J.D. Clogston, S.E. McNeil, Analyzing the influence of PEG molecular weight on the separation of PEGylated gold nanoparticles by asymmetric-flow field-flow fractionation, Anal. Bioanal. Chem. 407 (2015) 8661–8672. https://doi.org/10.1007/s00216-015-9056-9.

[33] H. Hinterwirth, S.K. Wiedmer, M. Moilanen, A. Lehner, G. Allmaier, T. Waitz, W. Lindner, M. Lämmerhofer, Comparative method evaluation for size and size-distribution analysis of gold nanoparticles: Other Techniques, J. Sep. Sci. 36 (2013) 2952–2961. https://doi.org/10.1002/jssc.201300460.

[34] L. Calzolai, D. Gilliland, C.P. Garcìa, F. Rossi, Separation and characterization of gold nanoparticle mixtures by flow-field-flow fractionation, J. Chromatogr. A. 1218 (2011) 4234–4239. https://doi.org/10.1016/j.chroma.2011.01.017.

[35] H. Kato, A. Nakamura, N. Noda, Determination of size distribution of silica nanoparticles: A comparison of scanning electron microscopy, dynamic light scattering, and flow field-flow fractionation with multiangle light scattering methods, Mater. Express. 4 (2014) 144–152. https://doi.org/10.1166/mex.2014.1150.

[36] J. Lohrke, A. Briel, K. Mäder, Characterization of superparamagnetic iron oxide nanoparticles by asymmetrical flow-field-flow-fractionation, Nanomed. 3 (2008) 437–452. https://doi.org/10.2217/17435889.3.4.437.

[37] G. Rigaux, C.V. Gheran, M. Callewaert, C. Cadiou, S.N. Voicu, A. Dinischiotu, M.C. Andry, L. Vander Elst, S. Laurent, R.N. Muller, A. Berquand, M. Molinari, S. Huclier-Markai, F. Chuburu, Characterization of Gd loaded chitosan-TPP nanohydrogels by a multi-technique approach

combining dynamic light scattering (DLS), asymetrical flow-field-flow-fractionation (AF4) and atomic force microscopy (AFM) and design of positive contrast agents for molecular resonance imaging (MRI), Nanotechnology. 28 (2017) 055705. https://doi.org/10.1088/1361-6528/aa5188.

[38] A. Gennari, J.M. Rios de la Rosa, E. Hohn, M. Pelliccia, E. Lallana, R. Donno, A. Tirella, N. Tirelli, The different ways to chitosan/hyaluronic acid nanoparticles: templated vs direct complexation. Influence of particle preparation on morphology, cell uptake and silencing efficiency, Beilstein J. Nanotechnol. 10 (2019) 2594–2608. https://doi.org/10.3762/bjnano.10.250.

[39] P.L. Ma, M.D. Buschmann, F.M. Winnik, One-Step Analysis of DNA/Chitosan Complexes by Field-Flow Fractionation Reveals Particle Size and Free Chitosan Content, Biomacromolecules. 11 (2010) 549–554. https://doi.org/10.1021/bm901345q.

[40] L.M. Forero Ramirez, E. Gobin, R. Aid-Launais, C. Journe, F.C. Moraes, L. Picton, D. Le Cerf, D. Letourneur, C. Chauvierre, F. Chaubet, Gd(DOTA)-grafted submicronic polysaccharide-based particles functionalized with fucoidan as potential MR contrast agent able to target human activated platelets, Carbohydr. Polym. 245 (2020) 116457. https://doi.org/10.1016/j.carbpol.2020.116457.

[41] R. Xu, Light scattering: A review of particle characterization applications, Particuology. 18 (2015) 11–21. https://doi.org/10.1016/j.partic.2014.05.002.

[42] C. Fuentes, J. Choi, C. Zielke, J.M. Peñarrieta, S. Lee, L. Nilsson, Comparison between conventional and frit-inlet channels in separation of biopolymers by asymmetric flow field-flow fractionation, The Analyst. 144 (2019) 4559–4568. https://doi.org/10.1039/C9AN00466A.

[43] J.Calvin. Giddings, Hydrodynamic relaxation and sample concentration in field-flow fractionation using permeable wall elements, Anal. Chem. 62 (1990) 2306–2312. https://doi.org/10.1021/ac00220a010.

[44] M.Kuang. Liu, P.Stephen. Williams, M.N. Myers, J.Calvin. Giddings, Hydrodynamic relaxation in flow field-flow fractionation using both split and frit inlets, Anal. Chem. 63 (1991) 2115–2122. https://doi.org/10.1021/ac00019a010.

[45] U. Till, M. Gaucher, B. Amouroux, S. Gineste, B. Lonetti, J.-D. Marty, C. Mingotaud, C.R.M. Bria, S.K.R. Williams, F. Violleau, A.-F. Mingotaud, Frit inlet field-flow fractionation techniques for the characterization of polyion complex self-assemblies, J. Chromatogr. A. 1481 (2017) 101–110. https://doi.org/10.1016/j.chroma.2016.12.050.

[46] G. Yohannes, M. Jussila, K. Hartonen, M.-L. Riekkola, Asymmetrical flow field-flow fractionation technique for separation and characterization of biopolymers and bioparticles, J. Chromatogr. A. 1218 (2011) 4104–4116. https://doi.org/10.1016/j.chroma.2010.12.110.

[47] T. Kowalkowski, B. Buszewski, C. Cantado, F. Dondi, Field-Flow Fractionation: Theory, Techniques, Applications and the Challenges, Crit. Rev. Anal. Chem. 36 (2006) 129–135. https://doi.org/10.1080/10408340600713702.

[48] W. Fraunhofer, G. Winter, The use of asymmetrical flow field-flow fractionation in pharmaceutics and biopharmaceutics, Eur. J. Pharm. Biopharm. 58 (2004) 369–383. https://doi.org/10.1016/j.ejpb.2004.03.034.

[49] M. Wagner, S. Holzschuh, A. Traeger, A. Fahr, Ulrich.S. Schubert, Asymmetric Flow Field-Flow Fractionation in the Field of Nanomedicine, Anal. Chem. 86 (2014) 5201–5210. https://doi.org/10.1021/ac501664t.

589 [50] J.C. Giddings, Retention (steric) inversion in field-flow fractionation: practical implications in
590 particle size, density and shape analysis, The Analyst. 118 (1993) 1487.
591 https://doi.org/10.1039/an9931801487.

592 [51] J.Calvin. Giddings, M.Hee. Moon, P.Stephen. Williams, M.N. Myers, Particle size distribution by
593 sedimentation/steric field-flow fractionation: development of a calibration procedure based on
594 density compensation, Anal. Chem. 63 (1991) 1366–1372.
595 https://doi.org/10.1021/ac00014a006.

596 [52] H. Dou, Y.-J. Lee, E.C. Jung, B.-C. Lee, S. Lee, Study on steric transition in asymmetrical flow
597 field-flow fractionation and application to characterization of high-energy material, J.
598 Chromatogr. A. 1304 (2013) 211–219. https://doi.org/10.1016/j.chroma.2013.06.051.

599 [53] Y.B. Kim, J.S. Yang, M.H. Moon, Investigation of steric transition with field programming in frit
600 inlet asymmetrical flow field-flow fractionation, J. Chromatogr. A. 1576 (2018) 131–136.
601 https://doi.org/10.1016/j.chroma.2018.09.036.

602 [54] M.H. Moon, H. Kwon, I. Park, Stopless Flow Injection in Asymmetrical Flow Field-Flow
603 Fractionation Using a Frit Inlet, Anal. Chem. 69 (1997) 1436–1440.
604 https://doi.org/10.1021/ac960897b.

605 [55] M. Hee Moon, P.S. Williams, D. Kang, I. Hwang, Field and flow programming in frit-inlet
606 asymmetrical flow field-flow fractionation, J. Chromatogr. A. 955 (2002) 263–272.
607 https://doi.org/10.1016/S0021-9673(02)00226-1.

608 [56] L. Calzolai, D. Gilliland, C.P. Garcìa, F. Rossi, Separation and characterization of gold
609 nanoparticle mixtures by flow-field-flow fractionation, J. Chromatogr. A. 1218 (2011) 4234–
610 4239. https://doi.org/10.1016/j.chroma.2011.01.017.

611 [57] M. Hansen, M.C. Smith, R.M. Crist, J.D. Clogston, S.E. McNeil, Analyzing the influence of PEG
612 molecular weight on the separation of PEGylated gold nanoparticles by asymmetric-flow field-
613 flow fractionation, Anal. Bioanal. Chem. 407 (2015) 8661–8672.
614 https://doi.org/10.1007/s00216-015-9056-9.

615 [58] M.-H. Jang, S. Lee, Y.S. Hwang, Characterization of Silver Nanoparticles under Environmentally
616 Relevant Conditions Using Asymmetrical Flow Field-Flow Fractionation (AF4), PLOS ONE. 10
617 (2015) e0143149. https://doi.org/10.1371/journal.pone.0143149.

618 [59] C. Cascio, D. Gilliland, F. Rossi, L. Calzolai, C. Contado, Critical Experimental Evaluation of Key
619 Methods to Detect, Size and Quantify Nanoparticulate Silver, Anal. Chem. 86 (2014) 12143–
620 12151. https://doi.org/10.1021/ac503307r.

621 [60] S. Bhattacharjee, DLS and zeta potential – What they are and what they are not?, J. Controlled
622 Release. 235 (2016) 337–351. https://doi.org/10.1016/j.jconrel.2016.06.017.

623 [61] A. Schädlich, C. Rose, J. Kuntsche, H. Caysa, T. Mueller, A. Göpferich, K. Mäder, How stealthy
624 are PEG-PLA nanoparticles? An NIR in vivo study combined with detailed size measurements,
625 Pharm. Res. 28 (2011) 1995–2007. https://doi.org/10.1007/s11095-011-0426-5.

626

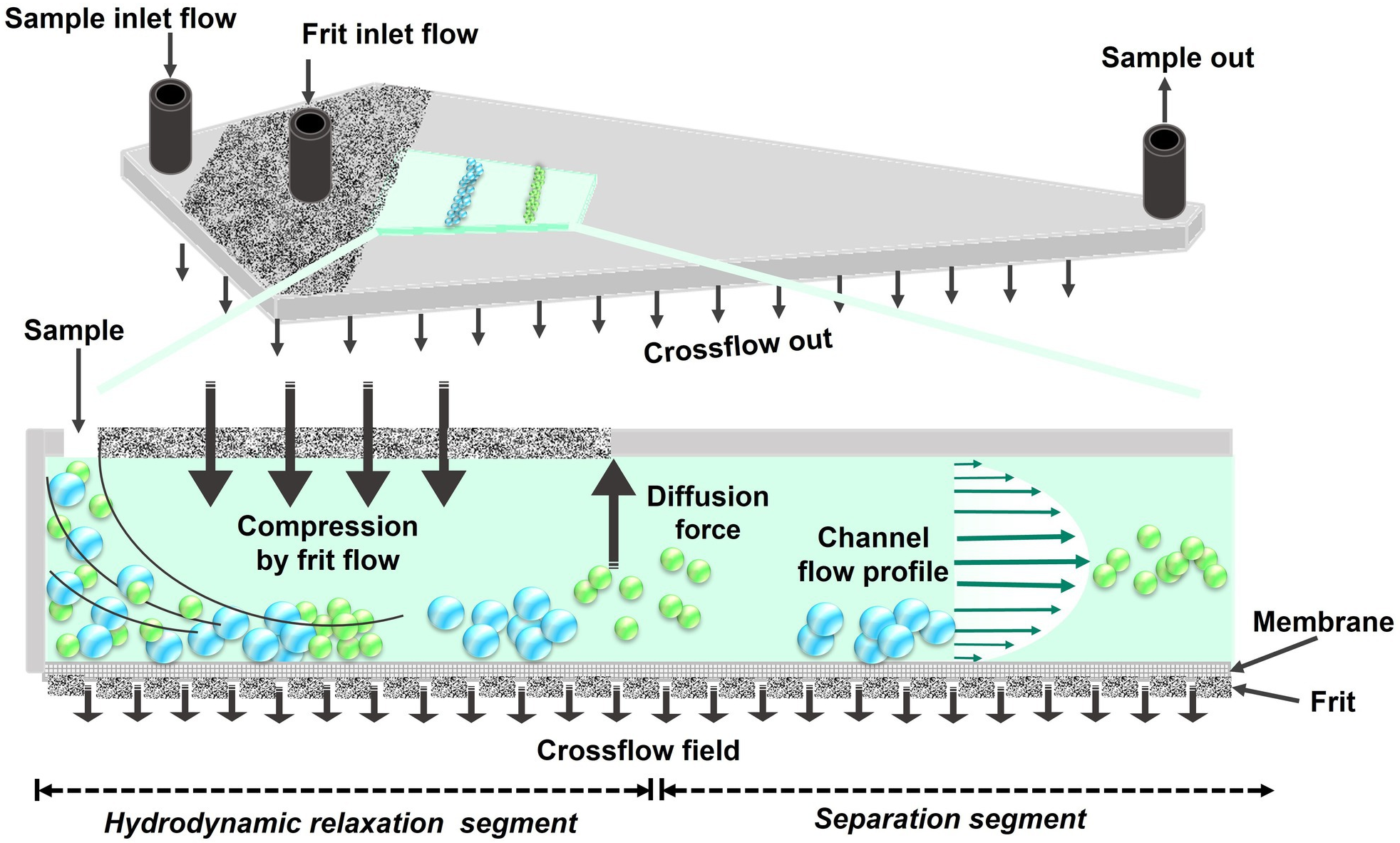
Sample inlet flow
Frit inlet flow
Sample out
Sample
Crossflow out
Compression
by frit flow
Diffusion
force
Channel
flow profile
Membrane
Frit
Crossflow field
Hydrodynamic relaxation segment
Separation segment

A

Dextran-NPs

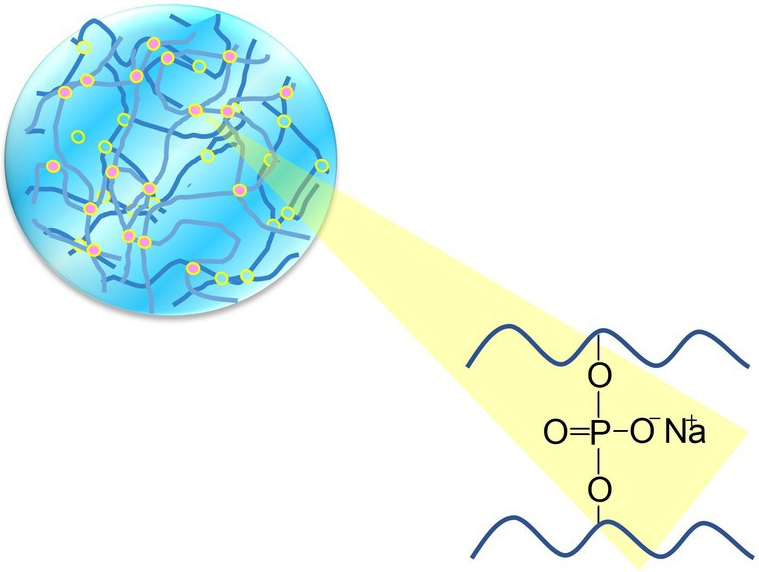


B

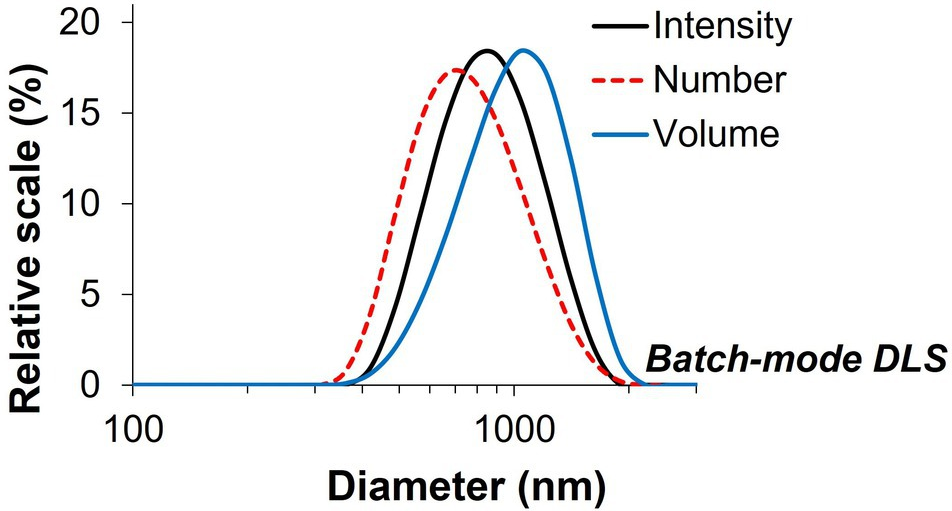


C

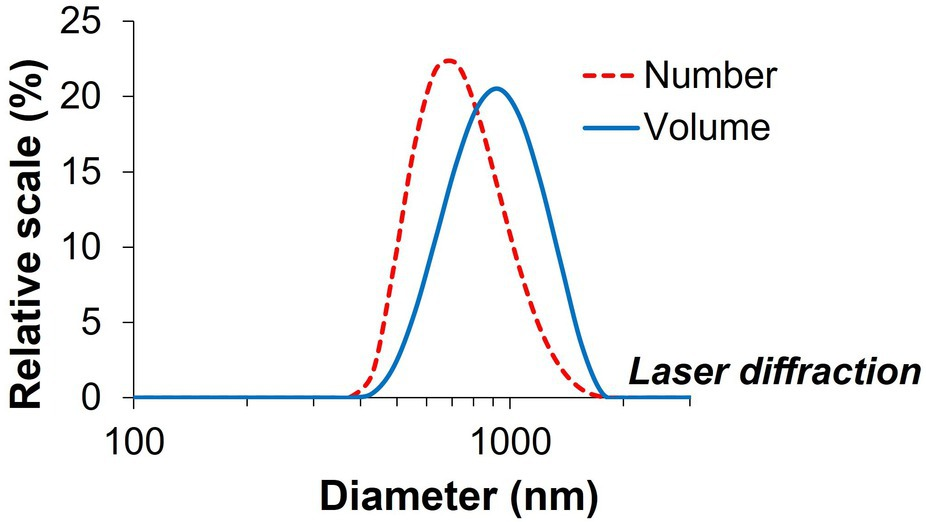

Figure 3 (Forero Ramirez et al) – revised

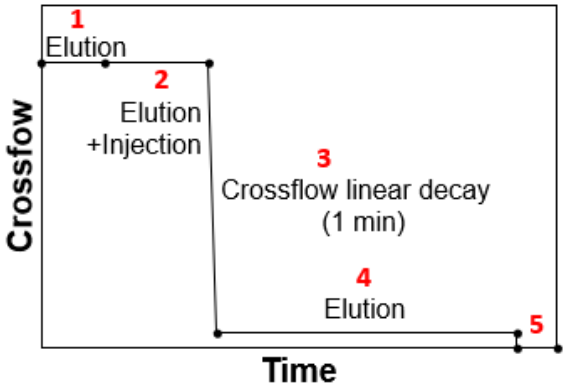


**Figure 3.** Schematic representation of FI-AF4 flow method. Samples were injected at a NPs concentration of 0.5 mg/mL (10 µL injection volume). Detector flow was held constant at 0.6 mL/min and the NPs were injected at 0.1 mL/min. A spacer thickness of 490 µm was used.

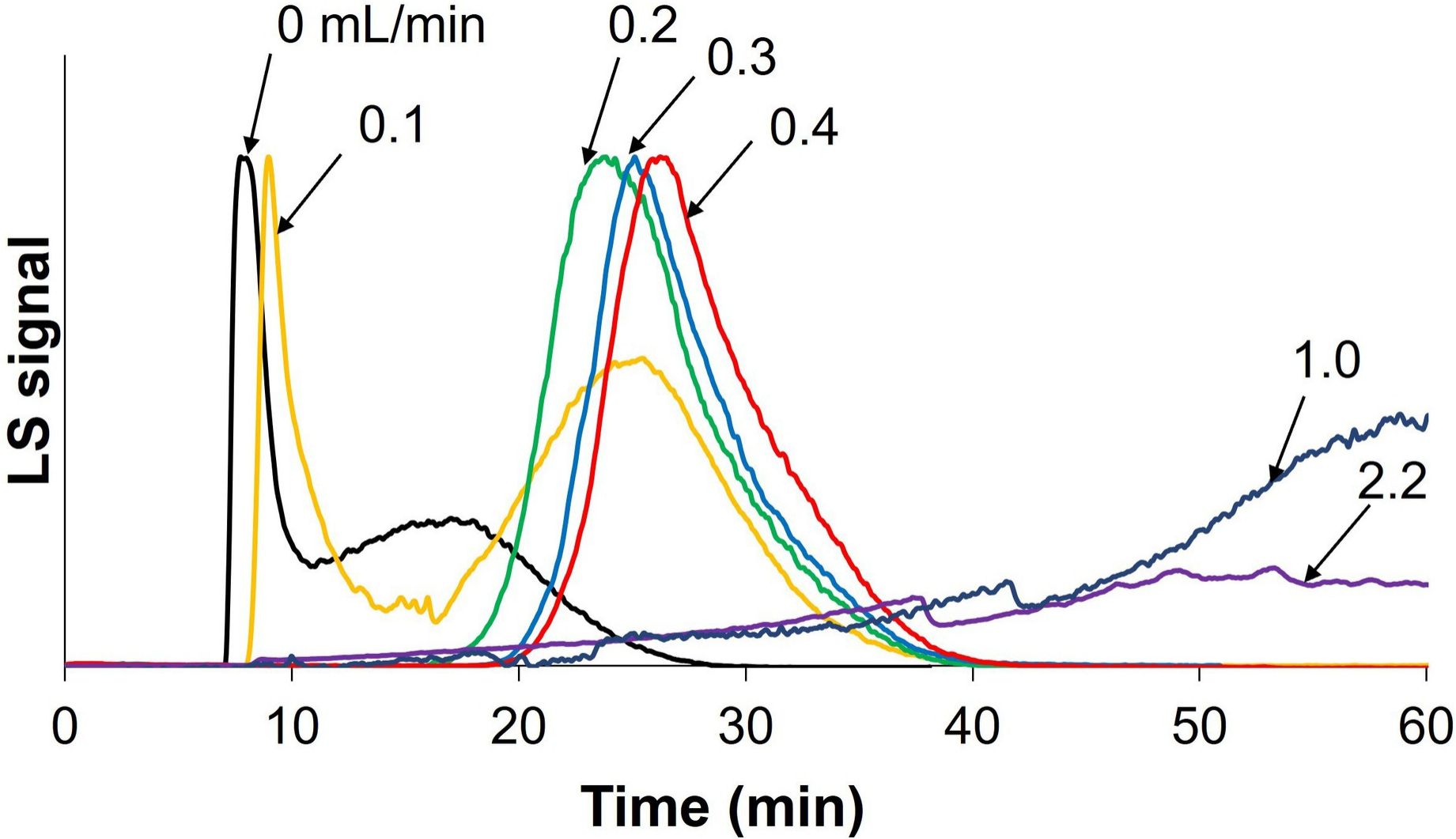
0 mL/min
0.1
0.2
0.3
0.4
1.0
2.2
LS signal
0
10
20
30
40
50
60
Time (min)

Figure 5 (Forero Ramirez et al) revised

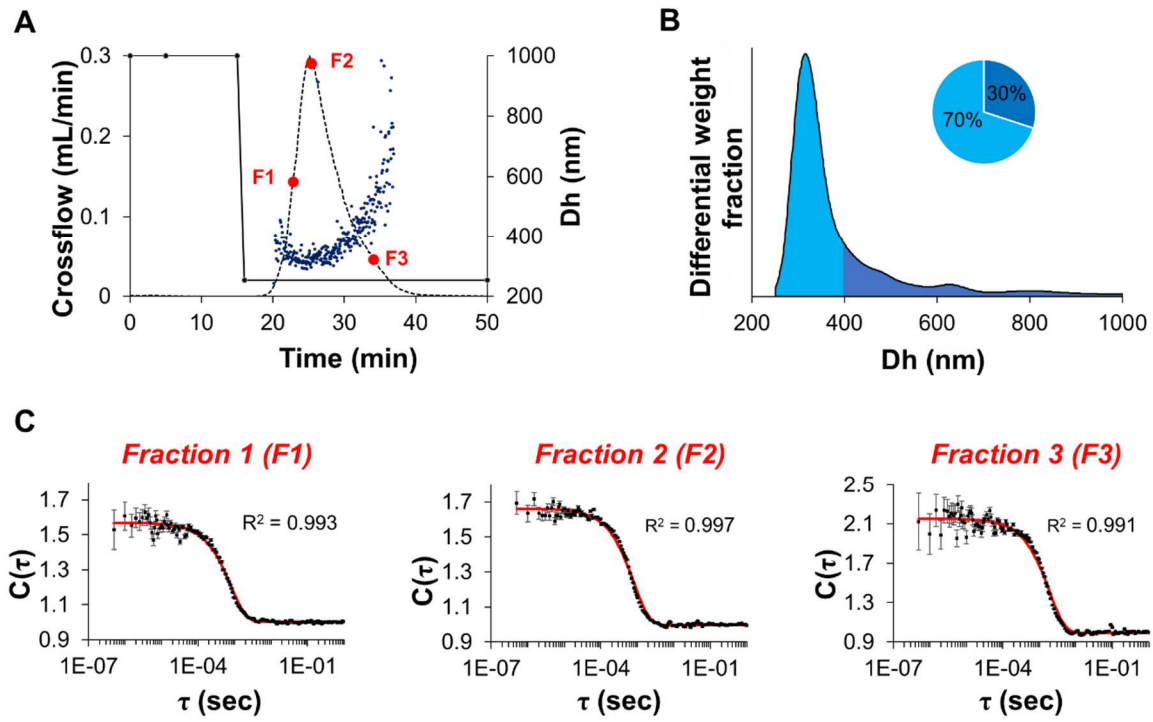


**Figure 5**. Size characterization of dextran-NPs by FI-AF4 coupled with DLS detector. (A) DLS fractogram and size distribution profile, (B) Weight~~Number~~-based distribution and (C) DLS correlation function plot of particles fractions recovered at different times as indicated on (A).

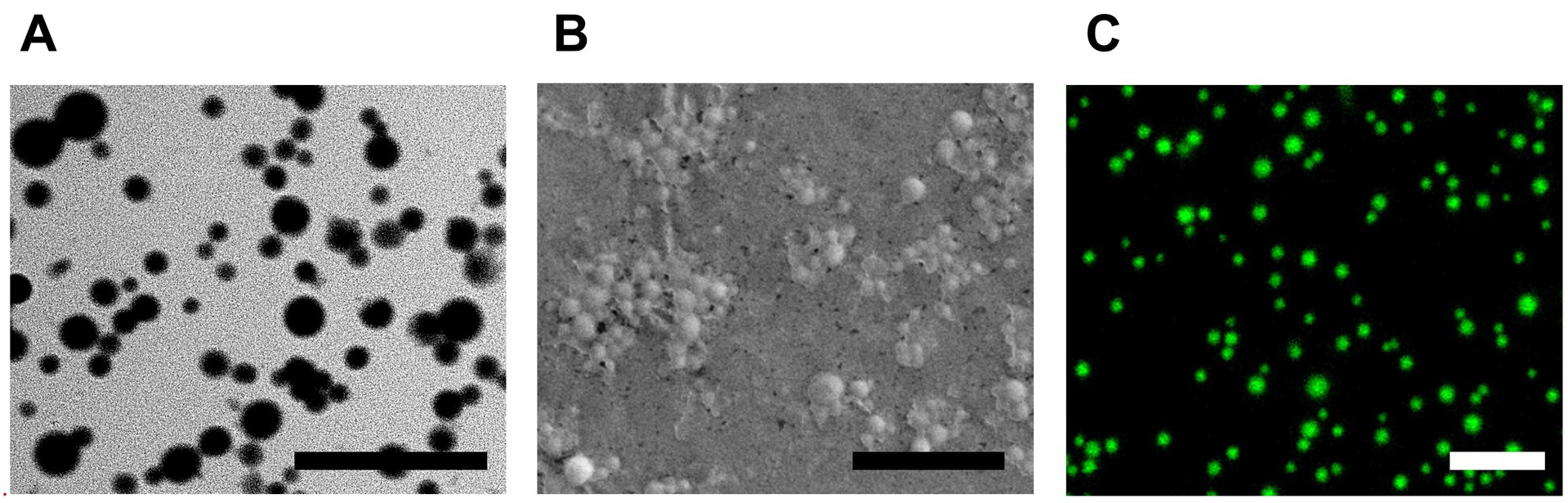
A
B
C

Figure 7 (Forero Ramirez et al) revised

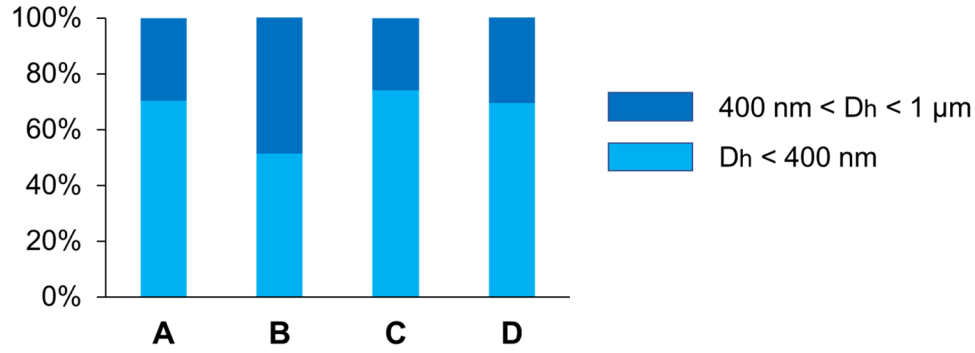


**Figure 7.** Weight~~Number~~-based PSD obtained by FI-AF4 for four independent batches of dextran-NPs prepared under the same experimental conditions.